

Article

A Two-LED Based Indoor Three-Dimensional Visible Light Positioning and Orienteering Scheme for a Tilted Receiver

Xiaodi You ^{1,*} , Xiaobai Yang ¹, Zile Jiang ² and Shuang Zhao ¹

¹ School of Electronic and Information Engineering, Soochow University, Suzhou 215006, China; 20205228029@stu.suda.edu.cn (X.Y.); szhaoszhao@stu.suda.edu.cn (S.Z.)

² Kuang Yaming Honors School, Nanjing University, Nanjing 210023, China; 181240026@smail.nju.edu.cn

* Correspondence: xdyou@suda.edu.cn

Abstract: Conventional visible light positioning (VLP) systems usually require at least three light-emitting diodes (LEDs) to enable trilateration or triangulation, which is infeasible when the LED condition is constrained. In this paper, we propose a novel indoor three-dimensional (3D) VLP and orienteering (VLPO) scheme. By using only two LEDs and two photo-detectors (PDs), our scheme can achieve simultaneous 3D localization and receiver orientation estimation efficiently. Further, to eliminate the location uncertainty caused by receiver tilt, we propose a location selection strategy which can effectively determine the true location of the receiver. Through extensive simulations, it is found that when the receiver faces upwards, the proposed scheme can achieve a mean 3D positioning error of 7.4 cm and a mean azimuthal error of 7.0°. Moreover, when the receiver tilts with a polar angle of 10°, accurate VLPO can still be achieved with 90.3% of 3D positioning errors less than 20 cm and 92.6% of azimuthal errors less than 5°. These results indicate that our scheme is a promising solution to achieve accurate VLPO when there is only two LEDs. Results also verify the effectiveness of the VLPO scheme when locating a tilted receiver.

Keywords: visible light positioning (VLP); three-dimensional (3D); visible light positioning and orienteering (VLPO); light-emitting diode (LED)



Citation: You, X.; Yang, X.; Jiang, Z.; Zhao, S. A Two-LED Based Indoor Three-Dimensional Visible Light Positioning and Orienteering Scheme for a Tilted Receiver. *Photonics* **2022**, *9*, 159. <https://doi.org/10.3390/photonics9030159>

Received: 30 January 2022

Accepted: 3 March 2022

Published: 5 March 2022

Publisher's Note: MDPI stays neutral with regard to jurisdictional claims in published maps and institutional affiliations.



Copyright: © 2022 by the authors. Licensee MDPI, Basel, Switzerland. This article is an open access article distributed under the terms and conditions of the Creative Commons Attribution (CC BY) license (<https://creativecommons.org/licenses/by/4.0/>).

1. Introduction

The emerging location-based services (LBSs) have raised increasing interest in localization technologies [1]. Satellite-based global positioning systems are widely used in outdoor environments. However, satellite signals suffer from fading when passing through solid walls, thus their positioning accuracy will be severely influenced in indoor environments such as underground parking, tunnels, and office buildings surrounded by skyscrapers. With the development of visible light communication (VLC) technologies, the visible light positioning (VLP) system using light-emitting diodes (LEDs) has been considered as a potential candidate for the next-generation indoor positioning system, due to its advantages of high accuracy, high efficiency, and low cost [2,3]. By modulating signals to existing lighting facilities, VLP systems can offer various indoor LBSs such as high-accurate indoor navigation, asset tracking, and autonomous robot control.

The simplest indoor VLP scheme is based on the principle of proximity and its positioning accuracy is usually in meters [4]. To improve the positioning accuracy, different VLP schemes based on trilateration or triangulation were reported, which can achieve centimeter-level VLP [5–7]. However, to offer positioning information for trilateration or triangulation, conventional VLP systems usually require at least three LEDs as transmitters to convey VLP signals according to the time domain multiplexing (TDM) or frequency domain multiplexing (FDM) protocols to avoid mutual interference at the receiver and make it easy for the receiver to distinguish between VLP signals [8,9]. Thus, at least three time slots or frequency bands are allocated for VLP. Since the bandwidth of off-the-shelf LEDs is narrow

and usually a few of tens of MHz [10], VLP will inevitably limit the available bandwidth of VLC in an integrated VLC and VLP system [11]. To ensure the ample capacity of VLC, new approaches are required to reduce the time or frequency resources allocated for VLP. This study will focus on the VLP mechanism to propose a new VLP model and its corresponding strategies to support VLP with fewer bandwidth resources.

Another issue is that the LED condition of a VLP system could be constrained in some common scenarios, e.g.,: (i) when the LED number is insufficient, i.e., less than three; and (ii) when LED lamps are installed along a straight line, e.g., in a corridor or a tunnel. In these scenarios, the receiver is likely to detect the VLP signals from only one or two LEDs. Thus, conventional VLP schemes based on trilateration or triangulation cannot be directly applied. Different approaches have been proposed to perform indoor VLP with less than three LEDs, which can be categorized as two-dimensional (2D) [12–14] or three-dimensional (3D) [15–17] schemes. However, all these schemes require additional equipment such as a camera [12,13,15], a mirror [14], line lasers [16], or at least three PDs [17], which could increase the system complexity and needs to be simplified. Motivated by this, this work will particularly focus on the 3D VLP scheme, which requires fewer PDs when the LED condition is constrained.

Recently, receiver orientation estimation has become an additional function of VLP. Joint VLP and orientation estimation schemes were proposed in [18,19], and they both support only 2D VLP with quite a number of LEDs (e.g., twenty LEDs in [18], and forty-eight LEDs in [19]). However, there have been no related works specifically dedicated to VLP schemes that can support simultaneous 3D localization and receiver orienteering using less than three LEDs and a PD-based receiver. Therefore, this work will also try to fill in the gap.

In this paper, we propose a novel indoor 3D VLP and orienteering (VLPO) scheme using two LEDs and a pair of PDs. To the best of our knowledge, this is the first time that a two-LED-two-PD-based indoor 3D VLPO scheme is proposed, by which only two time slots or frequency bands are required to convey VLP signals. Thus, the bandwidth resources allocated for VLP can be effectively reduced as compared with conventional schemes based on trilateration or triangulation. In addition, the proposed scheme can achieve a good trade-off between the system complexity and the localization capability. As shown in Table 1, by using two LEDs and two PDs without any other types of equipment, our scheme is the only one that supports simultaneous 3D VLP and orientation estimation for a tilted receiver, thus it can be considered as a promising solution, especially when the LED condition is constrained.

Table 1. Comparison between different VLP schemes.

Reference	Transmitter	Receiver	2D or 3D VLP	Support Orienteering	Support Receiver Tilt
[12]	2 LEDs	1 camera	2D	No	No
[13]	1 LED	1 camera	2D	No	No
[14]	2 LEDs	1 PD + 1 mirror	2D	No	No
[15]	1 LED	1 camera	3D	No	Yes
[16]	2 line lasers	2 PDs	3D	Yes	No
[17]	1 LED array	3 PDs	3D	No	Yes
[18]	20 LEDs	1 PD	2D	Yes	No
[19]	48 LEDs	7 PDs	2D	Yes	Yes
This work	2 LEDs	2 PDs	3D	Yes	Yes

The concept of the VLPO scheme was shown in our conference paper [20], wherein we have preliminarily verified its feasibility assuming the receiver to face upwards. However, when the receiver tilts, the model in [20] cannot be directly applied and needs to be modified. Therefore, in this work, we further develop the VLPO scheme by considering the scenario of a tilted receiver. To eliminate the potential location uncertainty caused by the receiver tilt, we propose a new location selection strategy for the VLPO system to determine the

true location of the receiver. We conduct extensive simulations to evaluate the positioning accuracy and orienteering accuracy in a $3\text{ m} \times 5\text{ m} \times 3\text{ m}$ indoor space. The influence from the interval between PDs, the ranging error between LEDs and PDs, and the polar angle of the tiled receiver is also evaluated. Results show that the proposed scheme is efficient to achieve accurate 3D VLPO when the LED condition is constrained. Specifically, when the receiver faces upwards, the proposed scheme can achieve a mean 3D positioning error of 7.4 cm and a mean azimuthal error of 7.0° . Moreover, when the receiver tilts with a polar angle of 10° , the proposed scheme can still achieve accurate VLP and orienteering, with 90.3% of 3D positioning errors less than 20 cm and 92.6% of azimuthal errors less than 5° . Results also indicate that increasing the interval between PDs and reducing the ranging error between LEDs and PDs help enhance the accuracy of VLPO, and the receiver tilt only slightly degrades the performance of the VLPO scheme.

The rest of this paper is organized as follows. Section 2 presents the principle of the proposed 3D VLPO system in detail. Simulations and performance analyses are conducted in Section 3. Finally, we conclude the paper in Section 4.

2. Proposed VLPO Scheme

In this study, we assume a multi-cell VLPO system, in which there are multiple LEDs installed along a straight line in the ceiling, and mobile receivers are distributed at different indoor locations. The LEDs are divided into different groups in pairs to spatially form multiple VLPO cells. Based on this multi-cell configuration, we focus on VLPO within a single cell where a mobile receiver can only detect the VLP signals emitted from two LEDs (LED_1 and LED_2). Without loss of generality, we abstract the receiver into a line segment and assume that a pair of photo-detectors (PD_1 and PD_2) are mounted on both ends of the receiver. Figure 1 shows the architecture of the proposed VLPO system. The 3D coordinates of LED_1 and LED_2 are (x_{t1}, y_{t1}, z_{t1}) and (x_{t2}, y_{t2}, z_{t2}) , respectively, which are a priori knowledge at the receiver. The 3D coordinates of PD_1 and PD_2 are (x_{r1}, y_{r1}, z_{r1}) and (x_{r2}, y_{r2}, z_{r2}) , respectively, which are unknown at the receiver and need to be estimated. We use the midpoint of PD_1 and PD_2 to represent the location of the receiver, i.e., $(x_R, y_R, z_R) = ((x_{r1} + x_{r2})/2, (y_{r1} + y_{r2})/2, (z_{r1} + z_{r2})/2)$. We also define the direction pointing from PD_1 towards PD_2 as the orientation of the receiver. Thus, the azimuthal angle of the receiver is defined by the angular rotation η ($-180^\circ < \eta \leq 180^\circ$) from the positive X-axis to the projection of the receiver (from PD_1 to PD_2) on the XY-plane. Therefore, if we successfully estimate the 3D coordinates of PD_1 and PD_2 , then the location and the orientation of the receiver can be calculated.

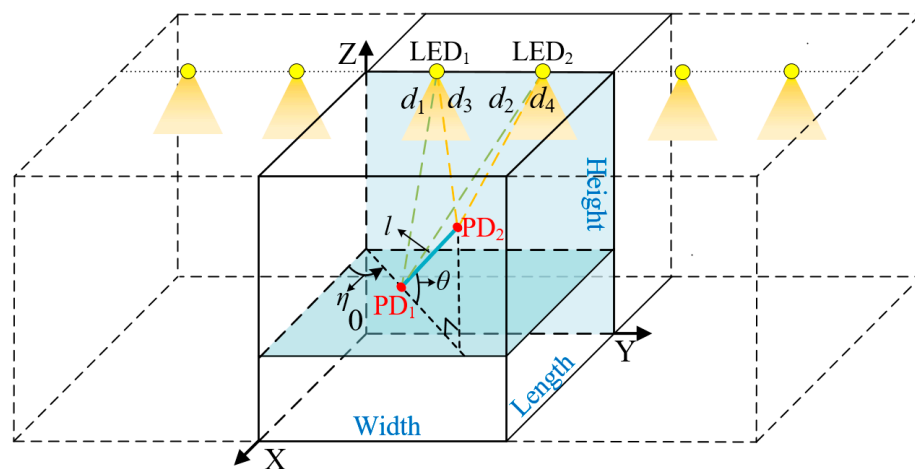


Figure 1. Proposed VLPO system.

To estimate the coordinates of PD_1 and PD_2 , we assume that the LEDs and PDs are perfectly synchronized to a common clock, and the VLP signals launched by the LEDs are used as the basis of ranging. Based on the ranging methods of time-of-arrival

(TOA) or phase-difference-of-arrival (PDOA) [21,22], the distances between the two LEDs and two PDs can be measured, and their estimation accuracy is typically in the order of centimeters [21]. We define the real distance between LED₁ and PD₁, LED₂ and PD₁, LED₁ and PD₂, LED₂ and PD₂ to be $d_1, d_2, d_3,$ and $d_4,$ respectively. Therefore, we obtain the following geometrical relationships:

$$\hat{d}_1^2 = (\hat{x}_{r1} - x_{t1})^2 + (\hat{y}_{r1} - y_{t1})^2 + (\hat{z}_{r1} - z_{t1})^2 \tag{1}$$

$$\hat{d}_2^2 = (\hat{x}_{r1} - x_{t2})^2 + (\hat{y}_{r1} - y_{t2})^2 + (\hat{z}_{r1} - z_{t2})^2 \tag{2}$$

$$\hat{d}_3^2 = (\hat{x}_{r2} - x_{t1})^2 + (\hat{y}_{r2} - y_{t1})^2 + (\hat{z}_{r2} - z_{t1})^2 \tag{3}$$

$$\hat{d}_4^2 = (\hat{x}_{r2} - x_{t2})^2 + (\hat{y}_{r2} - y_{t2})^2 + (\hat{z}_{r2} - z_{t2})^2 \tag{4}$$

where \hat{d}_i ($i = 1, 2, 3, 4$) is the estimated values of d_i ($i = 1, 2, 3, 4$) obtained by ranging, $(\hat{x}_{r1}, \hat{y}_{r1}, \hat{z}_{r1})$ is the coordinate of PD₁ to be estimated, and $(\hat{x}_{r2}, \hat{y}_{r2}, \hat{z}_{r2})$ is the coordinate of PD₂ to be estimated. To offer richer information for performing VLPO, the interval between PD₁ and PD₂ is known at the receiver and fixed at l . Additionally, we assume that the polar angle θ ($0^\circ \leq \theta \leq 90^\circ$) of the tilted receiver can be acquired by extra sensors at the receiver [22]. When $\theta = 0^\circ$, the receiver faces upwards. Based on these presumptions, we can derive additional geometrical relationships:

$$l^2 = (\hat{x}_{r2} - \hat{x}_{r1})^2 + (\hat{y}_{r2} - \hat{y}_{r1})^2 + (\hat{z}_{r2} - \hat{z}_{r1})^2 \tag{5}$$

$$\hat{z}_{r2} = \hat{z}_{r1} + l \sin \theta \tag{6}$$

According to the above nonlinear system of equations from Equations (1)–(6), we expect to solve the coordinates of PD₁ and PD₂. However, it would be difficult to directly solve the coordinates of PDs from Equations (1)–(6) in the current XYZ-coordinate system. Thus, we divide the solving process into three steps, which includes establishing intersection circles, conducting coordinate transformations, and excluding redundant solutions.

Figure 2a shows the schematic diagram of establishing intersection circles. In this step, we first subtract between Equations (1) and (2), i.e., the two spherical surfaces centered at LED₁ and LED₂, to obtain a plane equation, which is described by a plane P₁. PD₁ is located in the plane P₁, specifically, on the intersection circle K₁ between the spherical surfaces Equations (1) and (2). Here, K₁ is centered at (a_1, b_1, c_1) with a radius of R_1 . Similarly, after subtracting between Equations (3) and (4), PD₂ is located in a plane P₂, specifically, on the intersection circle K₂ centered at (a_2, b_2, c_2) with a radius of R_2 . For the intersection circles K₁ and K₂, the coordinates of K_i ($i = 1, 2$) are given by:

$$K_i(a_i, b_i, c_i) = \left(x_{t1} + (x_{t2} - x_{t1}) \frac{w_i}{L}, y_{t1} + (y_{t2} - y_{t1}) \frac{w_i}{L}, z_{t1} + (z_{t2} - z_{t1}) \frac{w_i}{L} \right) \tag{7}$$

where L is the distance between LED₁ and LED₂, and w_i ($i = 1, 2$) is the distance from LED₁ to the Plane P_i ($i = 1, 2$), derived as:

$$w_1 = \frac{\left| (x_{t2} - x_{t1})^2 + (y_{t2} - y_{t1})^2 + (z_{t2} - z_{t1})^2 + \hat{d}_1^2 - \hat{d}_2^2 \right|}{2\sqrt{(x_{t2} - x_{t1})^2 + (y_{t2} - y_{t1})^2 + (z_{t2} - z_{t1})^2}} \tag{8}$$

$$w_2 = \frac{\left| (x_{t2} - x_{t1})^2 + (y_{t2} - y_{t1})^2 + (z_{t2} - z_{t1})^2 + \hat{d}_3^2 - \hat{d}_4^2 \right|}{2\sqrt{(x_{t2} - x_{t1})^2 + (y_{t2} - y_{t1})^2 + (z_{t2} - z_{t1})^2}} \tag{9}$$

Additionally, the radiuses R_i ($i = 1, 2$) of the intersection circles can be written by:

$$R_1 = \sqrt{\hat{d}_1^2 - w_1^2} \tag{10}$$

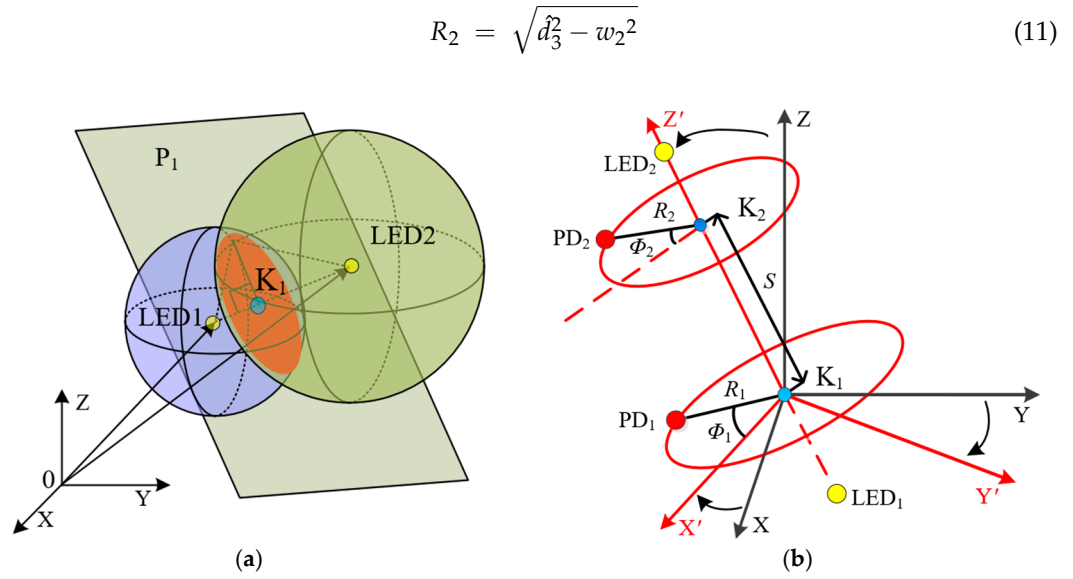


Figure 2. Schematic diagrams of the solving process: (a) establishing intersection circles; and (b) conducting coordinate transformations.

Now, based on the circles K_1 and K_2 , the solving process for the coordinates of PDs can be simplified by constructing new coordinate systems. Thus, in the second step, we conduct coordinate transformations, as shown in Figure 2b. We first transform the XYZ-coordinate system into the $X' Y' Z'$ -coordinate system, in which K_1 is the origin point, line K_1K_2 forms the Z' -axis, and the intersection line between the plane P_1 and the XY-plane forms the X' -axis. Next, we transform the $X' Y' Z'$ -coordinate system into the cylindrical coordinate system, in which the cylindrical coordinates of PD_1 and PD_2 are denoted by $(R_1, \Phi_1, 0)$ and (R_2, Φ_2, S) , respectively. Here, S is the distance between K_1 and K_2 . After coordinate transformations, Equations (5) and (6) can be written in the form of the cylindrical coordinates:

$$\Phi_1 - \Phi_2 = \pm \arccos M \tag{12}$$

$$\beta(R_2 \sin \Phi_2 - R_1 \sin \Phi_1) = l \sin \theta - \gamma S \tag{13}$$

where $M = (R_1^2 + R_2^2 + S^2 - l^2)/(2R_1R_2)$, $\beta = -\sqrt{(a^2+b^2)}/S$, $\gamma = c/S$, $a = a_2 - a_1$, $b = b_2 - b_1$, $c = c_2 - c_1$, and $S = \sqrt{a^2+b^2+c^2}$. By solving (12) and (13), Φ_1 and Φ_2 can be obtained. Then, we perform coordinate inverse transformations to recover the coordinates of PD_1 and PD_2 in the XYZ-coordinate system, which are, respectively, given by:

$$(\hat{x}_{r1}, \hat{y}_{r1}, \hat{z}_{r1})' = (e_x, e_y, e_z)(R_1 \cos \Phi_1, R_1 \sin \Phi_1, 0)' + (a_1, b_1, c_1)' \tag{14}$$

$$(\hat{x}_{r2}, \hat{y}_{r2}, \hat{z}_{r2})' = (e_x, e_y, e_z)(R_2 \cos \Phi_2, R_2 \sin \Phi_2, S)' + (a_1, b_1, c_1)' \tag{15}$$

Here, the orthonormal bases are given by $e_x = (b/\sqrt{a^2+b^2}, -a/\sqrt{a^2+b^2}, 0)'$, $e_y = [ac/(S\sqrt{(a^2+b^2)}), bc/(S\sqrt{(a^2+b^2)}), -\sqrt{(a^2+b^2)}/S]'$, and $e_z = (a/S, b/S, c/S)'$.

Based on the solving process from Equations (12)–(15), we get a total of four solutions. In other words, due to geometrical symmetry, a total of four pairs of the estimated coordinates of PD_1 and PD_2 are distributed in the space, among which only one is true. This means that the location of the receiver cannot be determined due to multiple solutions, and we call this situation as location uncertainty. To eliminate location uncertainty, the third step is to exclude the redundant solutions and get the true solution. In practice, the height of the VLP receiver is lower than the height of LED transmitters. Thus, we first exclude the solutions that are above the ceiling by setting the first constraint condition:

$(\hat{z}_{r1} + \hat{z}_{r2})/2 < \min(z_{t1}, z_{t2})$. Among the rest of solutions, we perform a further exclusion by considering the possible moving range of the receiver. In this study, we assume that the receiver moves within the constrained space on the outside of the YZ-plane by setting the second constraint condition: $\hat{x}_{r1} + \hat{x}_{r2} \geq 0$, which is shown in Figure 1.

During our study, we find that if the receiver faces upwards, i.e., the polar angle $\theta = 0^\circ$, then only one solution remains after considering the above two constraint conditions. This solution is taken as the estimated coordinates of PD₁ and PD₂, based on which the 3D location and the orientation of the receiver can be finally calculated. However, if the receiver tilts, i.e., $\theta \neq 0^\circ$, we may obtain one or two solutions remained after considering the above two constraint conditions, depending on the location of the receiver, the orientation of the receiver, and the ranging error between LEDs and PDs. Therefore, to eliminate the location uncertainty caused by the receiver tilt, we propose a location selection strategy to select the true location of PDs.

Figure 3 shows a flow chart of the location selection strategy. For a tilted receiver, if there remains only one pair of the estimated coordinates of PD₁ and PD₂, i.e., the case of one solution, then they can be directly used to perform VLPO for the receiver. However, if there remain two solutions, then we need to exclude the redundant solution by making comparisons between the received signal power at the PDs and the expected received signal power at the specific locations. Without loss of generality, we use the Solution A and the Solution A' to represent the two possible solutions remained, among which only one is true. For the Solution A, the estimated coordinates of PD₁ and PD₂ are, respectively, defined by $(x_{r1}^{es}, y_{r1}^{es}, z_{r1}^{es})$ and $(x_{r2}^{es}, y_{r2}^{es}, z_{r2}^{es})$, and for the Solution A', the estimated coordinates of PD₁ and PD₂ are, respectively, defined by $(x_{r1}^{es'}, y_{r1}^{es'}, z_{r1}^{es'})$ and $(x_{r2}^{es'}, y_{r2}^{es'}, z_{r2}^{es'})$.

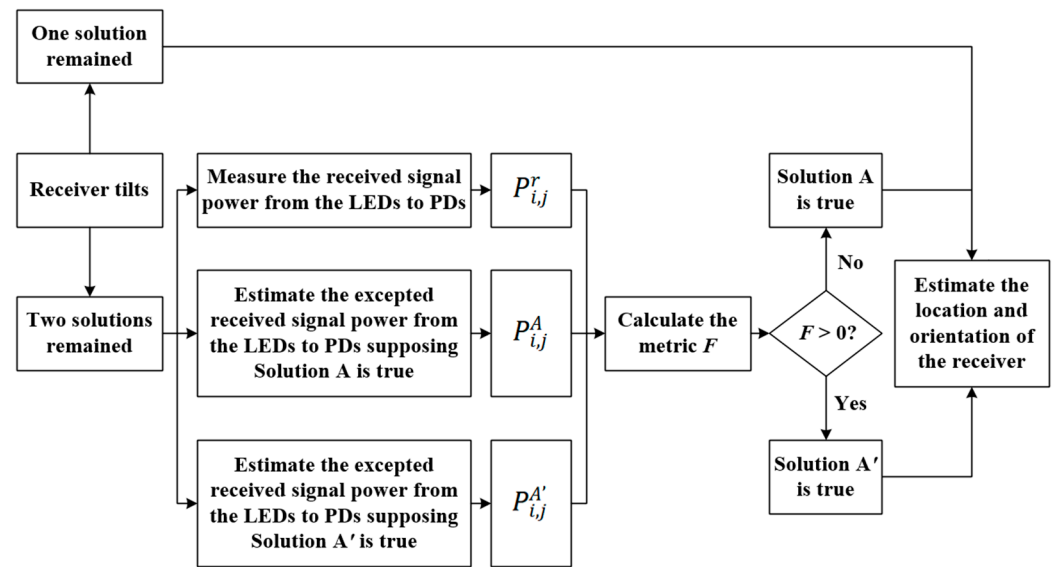


Figure 3. Flow chart of location selection strategy.

We first measure the received signal power from LED_{*i*} (*i* = 1, 2) to PD_{*j*} (*j* = 1, 2), which is expressed by:

$$P_{i,j}^r = \int_0^T s(t) \otimes h_{i,j}^{total}(t) dt / T \tag{16}$$

where $s(t)$ is the transmitted VLP signal, T is the duration of $s(t)$, and $h_{i,j}^{total}(t)$ is the total channel impulse response (CIR) from LED_{*i*} (*i* = 1, 2) to PD_{*j*} (*j* = 1, 2), which can be further written by [23,24]:

$$h_{i,j}^{total}(t) = h_{i,j}^{LOS}(t) + h_{i,j}^{NLOS}(t) = H_{i,j}^{LOS}(0) \delta(t - \tau_{i,j}^{LOS}) + \int_{\tau_{i,j}^{NLOS}=0}^{+\infty} A_{i,j}^{NLOS}(\tau_{i,j}^{NLOS}) \delta(t - \tau_{i,j}^{NLOS}) d\tau_{i,j}^{NLOS} \tag{17}$$

Here, $\delta(t)$ is Dirac function. From LED_{*i*} (*i* = 1, 2) to PD_{*j*} (*j* = 1, 2), $h_{i,j}^{LOS}(t)$ is the line-of-sight (LOS) CIR, $h_{i,j}^{NLOS}(t)$ is the non-LOS (NLOS) CIR, $\tau_{i,j}^{LOS}$ and $\tau_{i,j}^{NLOS}$ represent the signal time delays of the LOS and NLOS channels, respectively, $H_{i,j}^{LOS}(0)$ is the DC gain of the LOS channel, and $A_{i,j}^{NLOS}(\tau_{i,j}^{NLOS})$ is the gain of the NLOS channel with a time delay $\tau_{i,j}^{NLOS}$.

We assume all the LEDs have a Lambertian radiation pattern. Then, by supposing that the Solution A is true, we can estimate the expected received signal power from LED_{*i*} (*i* = 1, 2) to PD_{*j*} (*j* = 1, 2) based on the coordinates in Solution A, which is derived by [7,23]:

$$P_{i,j}^A = H_{i,j}^{LOS}(0) P_i^t = \frac{(m+1)A_r(z_{ti} - z_{rj}^{es})^{m+1} T_s g P_i^t}{2\pi \left((x_{ti} - x_{rj}^{es})^2 + (y_{ti} - y_{rj}^{es})^2 + (z_{ti} - z_{rj}^{es})^2 \right)^{(m+3)/2}} \quad (18)$$

where P_i^t is the transmitted power of LED_{*i*} (*i* = 1, 2), *m* is the Lambertian emission order of LEDs, A_r is the effective area of PDs, T_s is the gain of an optical filter, *g* is the gain of an optical concentrator. Similarly, by supposing that the Solution A' is true, we can also estimate the expected received signal power from LED_{*i*} (*i* = 1, 2) to PD_{*j*} (*j* = 1, 2) based on the coordinates in Solution A', which is derived by [7,23]:

$$P_{i,j}^{A'} = \frac{(m+1)A_r(z_{ti} - z_{rj}^{es'})^{m+1} T_s g P_i^t}{2\pi \left((x_{ti} - x_{rj}^{es'})^2 + (y_{ti} - y_{rj}^{es'})^2 + (z_{ti} - z_{rj}^{es'})^2 \right)^{(m+3)/2}} \quad (19)$$

Next, by comparing the power differences between $P_{i,j}^r$, $P_{i,j}^A$, and $P_{i,j}^{A'}$, we construct a metric *F* to determine the true solution, which is written as:

$$F = \sum_{j=1}^2 \sum_{i=1}^2 \left((P_{i,j}^r - P_{i,j}^A)^2 - (P_{i,j}^r - P_{i,j}^{A'})^2 \right) \quad (20)$$

If $F > 0$, then the Solution A' is selected as the true solution for the subsequent location and orientation estimation of the receiver; otherwise, the Solution A is selected.

Finally, by using the single solution remained, the 3D coordinate of the receiver is estimated by $(\hat{x}_R, \hat{y}_R, \hat{z}_R) = ((\hat{x}_{r1} + \hat{x}_{r2})/2, (\hat{y}_{r1} + \hat{y}_{r2})/2, (\hat{z}_{r1} + \hat{z}_{r2})/2)$, and its azimuthal angle η is estimated by:

$$\hat{\eta} = \text{sign}(\hat{y}_{r2} - \hat{y}_{r1}) \arccos \left[(\hat{x}_{r2} - \hat{x}_{r1}) / \sqrt{(\hat{x}_{r1} - \hat{x}_{r2})^2 + (\hat{y}_{r1} - \hat{y}_{r2})^2} \right] \quad (21)$$

where sign (·) represents sign function.

3. Simulation Results and Discussions

We evaluate the performance of the proposed VLPO scheme in a 3 m × 5 m × 3 m (length × width × height) indoor space based on the XYZ-coordinate system, as shown in Figure 1. In a considered VLPO cell, there are only two LED transmitters (LED₁ and LED₂) and a mobile receiver. LED₁ and LED₂ are located at (0, 1.5, 3) and (0, 3.5, 3), respectively, both of which have a Lambertian radiation pattern. Two PDs (PD₁ and PD₂) are mounted at both ends of the receiver to jointly estimate the location and the orientation of the receiver. Around the VLPO cell, there stands three walls, which are represented by three plane equations: (i) $x = 3, 0 \leq y \leq 5, 0 \leq z \leq 3$; (ii) $y = 0, 0 \leq x \leq 3, 0 \leq z \leq 3$; and (iii) $y = 5, 0 \leq x \leq 3, 0 \leq z \leq 3$. Thus, the channel between the LEDs and PDs consists of both LOS and NLOS channels, wherein the first indoor reflection is considered. We assume that the TOA ranging method is used to estimate the distances between the LEDs and PDs.

However, due to many factors including the geometry of the room, the frequency and transmitted power of the VLP signal, and the physical characteristics of LEDs and PDs, the distance estimation accuracy of the TOA method will be influenced [21]. Therefore, random estimation errors occur with respect to the real distances $d_1, d_2, d_3,$ and d_4 between LEDs and PDs. We assume these ranging errors are zero-mean, independent and identically Gaussian distributed, and they have the same standard deviation denoted as Δd . In our simulations, we assume that the receiver is located at certain test locations and the interval between adjacent test locations at the same height is 0.5 m. The receiver faces upwards ($\theta = 0^\circ$) in Figures 4–7, and can be tilted ($\theta > 0^\circ$) in Figures 8–11. The azimuthal angle of the receiver is randomly distributed in the range of $-180^\circ < \eta \leq 180^\circ$. To calculate the cumulative distribution functions (CDFs) of the positioning error and the azimuthal error, we conduct Monte Carlo simulations at least 50 times at each test location. Table 2 lists the key parameters of the indoor VLPO system. Other parameters of the receiver are the same as those in [23].

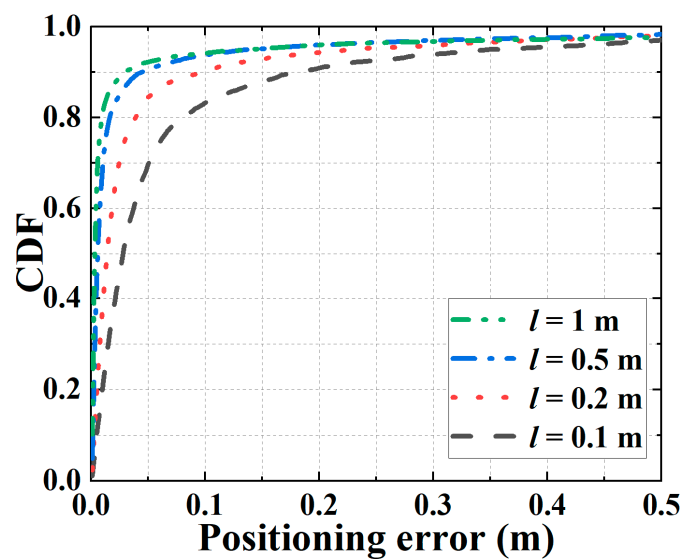


Figure 4. CDFs of 3D positioning errors at (0.5, 1, 1). ($\theta = 0^\circ$).

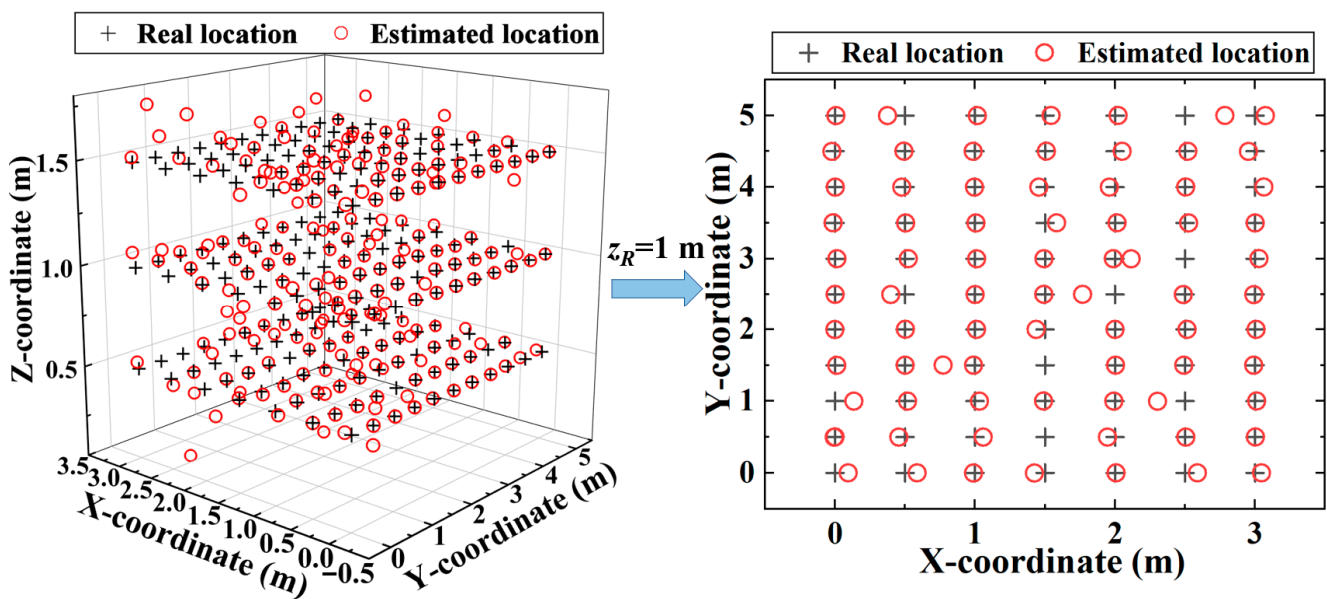


Figure 5. An example of 3D positioning results. ($\theta = 0^\circ$).

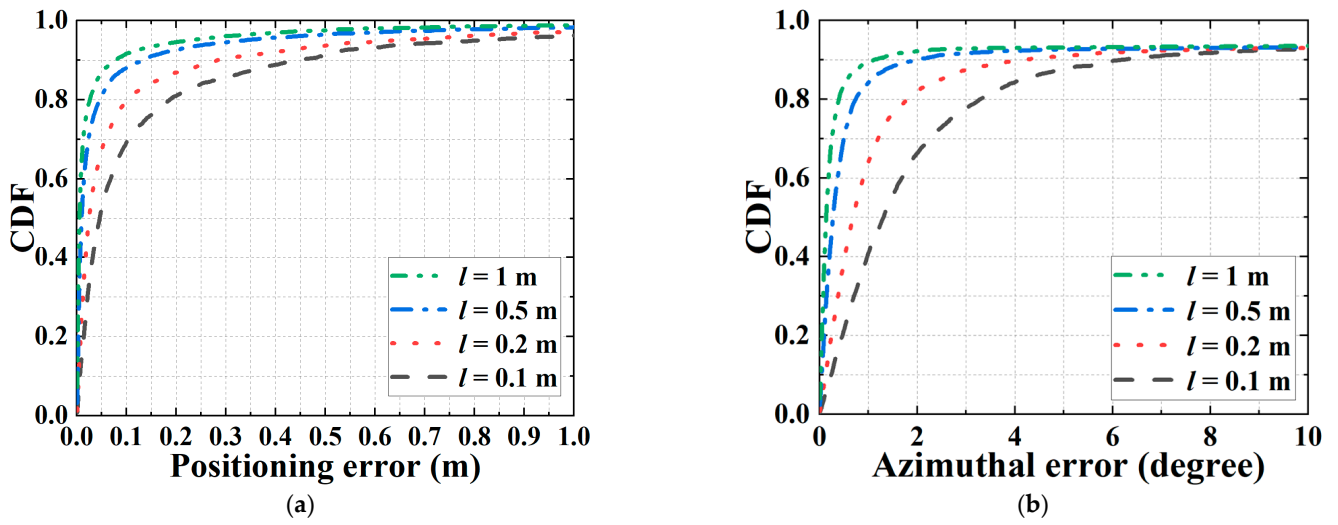


Figure 6. CDFs at the height of 1 m for: (a) 3D positioning errors; and (b) azimuthal errors. ($\theta = 0^\circ$).

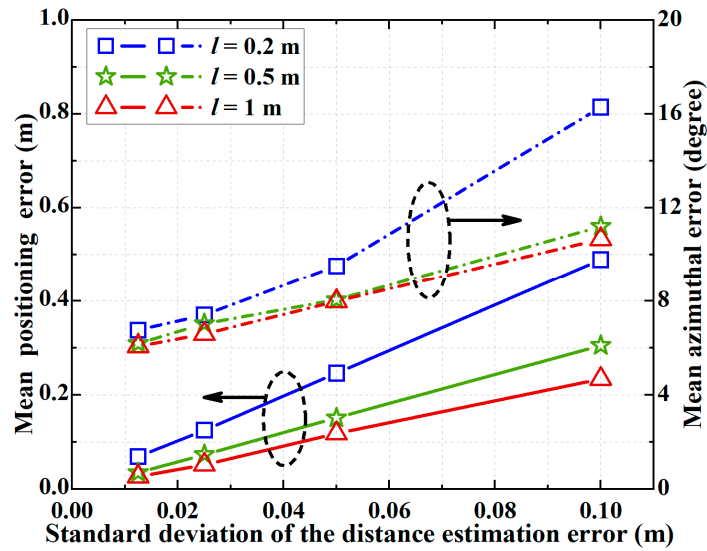


Figure 7. Mean positioning errors and azimuthal errors at the height of 1 m. ($\theta = 0^\circ$).

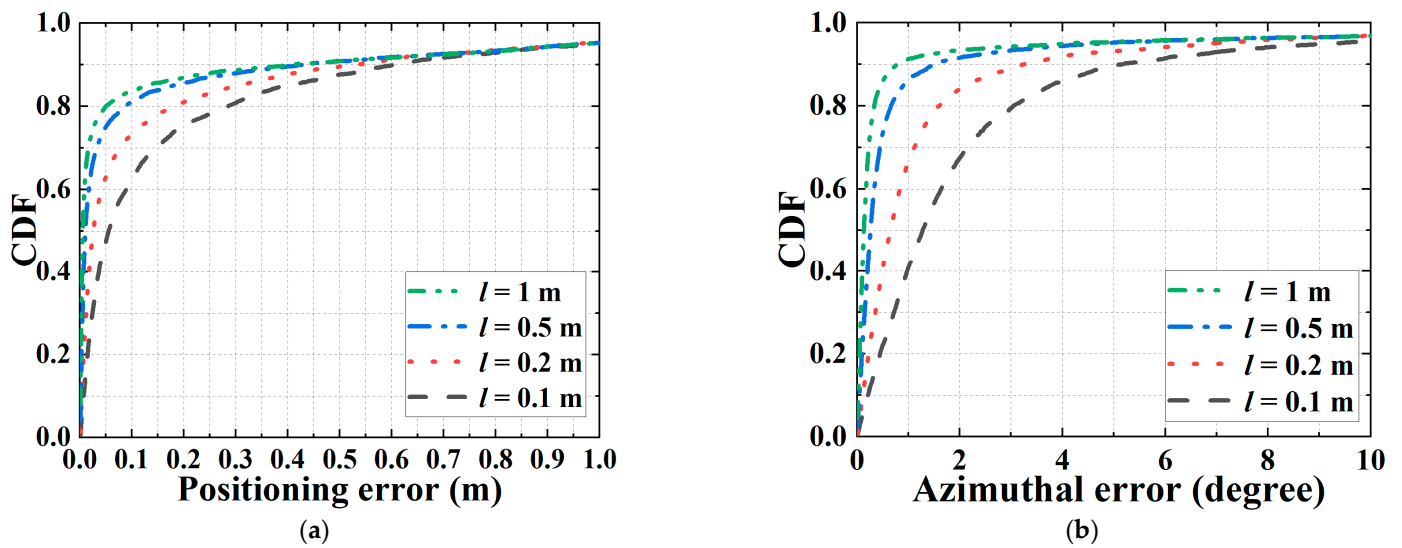


Figure 8. CDFs at (1.5, 2, 1) for: (a) 3D positioning errors; and (b) azimuthal errors. ($\theta = 30^\circ$).

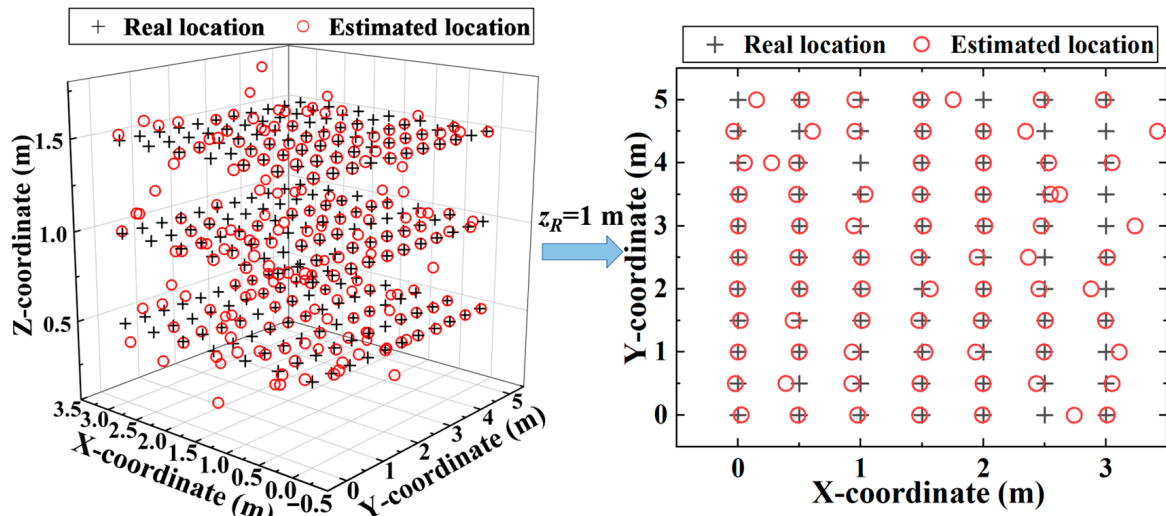


Figure 9. An example of 3D positioning results. ($\theta = 20^\circ$).

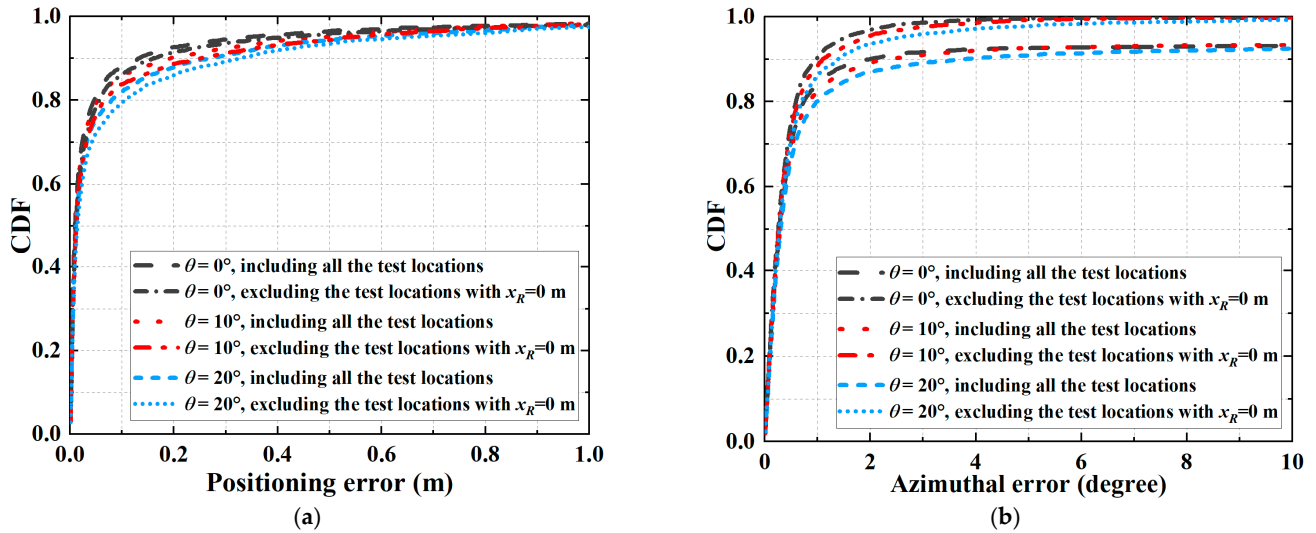


Figure 10. CDFs at the height of 1 m for: (a) 3D positioning errors; and (b) azimuthal errors. ($\theta = 0^\circ, 10^\circ$, and 20°).

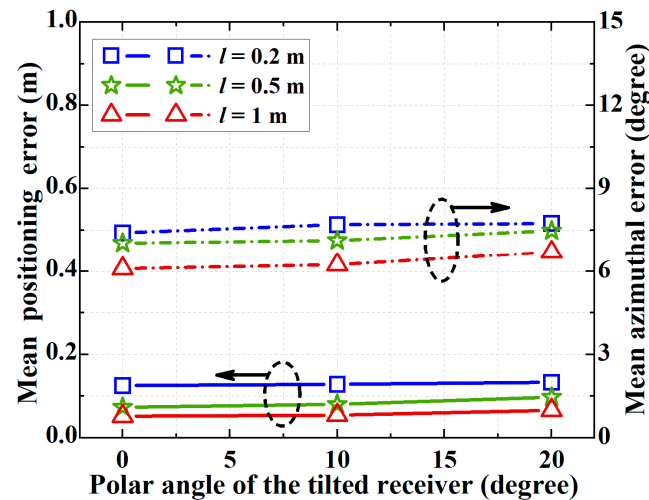


Figure 11. Mean positioning errors and azimuthal errors at the height of 1 m. ($\theta = 0^\circ, 10^\circ$, and 20°).

Table 2. Key parameters of the VLPO system.

Name of Parameters	Values
Indoor space (length × width × height)	3 m × 5 m × 3 m
Height of receiver	0.5 m/1 m/1.5 m
Launch power of each LED	5 Watt
Modulation index	0.1
Lambertian emission order of LEDs	1
LED semi-angle at half power	60°
Field-of-view (FOV) at the receiver	170°
Effective area of photo-detector	10 ⁻⁴ m ²
Photo-detector responsivity	0.35 A/W
Reflection coefficient of wall	0.83
Gain of the optical filter	1
Refractive index of the optical concentrator	1.5
Baud rate of the VLP signal	10 Msymbol/s

We first evaluate the performance of the VLPO scheme when the receiver faces upwards ($\theta = 0^\circ$). Figure 4 shows the simulated CDFs of the 3D positioning errors when the receiver is fixed at a specific location (0.5, 1, 1). Different curves represent the CDFs obtained by adopting different intervals l between PDs. We assume the standard deviation Δd of the ranging error is 0.025 m. We note that, when l is 0.1 m, 0.2 m, 0.5 m, and 1 m, the probability of achieving 3D positioning errors less than 10 cm is 83.2%, 90.2%, 93.7%, and 94.1%, respectively. This is because when Δd is fixed, adopting a larger l helps enhance the tolerance against the ranging error, thereby improving the positioning accuracy. Specifically, around 90% of 3D positioning errors are less than 9.8 cm when l is 0.2 m, and by further increasing l to 0.5 m, 90% of 3D positioning errors are less than 4.5 cm, thus verifying the high positioning accuracy of the proposed VLPO scheme when $\theta = 0^\circ$.

To evaluate the performance of the VLPO scheme at different locations, Figure 5 shows an example of 3D positioning results in different receiving planes at the height of 0.5 m, 1 m, and 1.5 m. Here, we assume that the interval between PDs is 0.2 m and the standard deviation of the ranging error is 0.025 m. We test 77 locations in each receiving plane, thus a total of 231 locations are tested for performance evaluation in the considered indoor space. We use “+” to represent the real locations of the receiver and “○” to represent the coordinates estimated from the proposed VLPO scheme. On the left of Figure 5, it can be observed that most of the estimated 3D locations are close to their corresponding real locations, thus verifying the effectiveness of the proposed VLPO scheme at different locations. By comparison, we find that the 3D positioning accuracy is related to the height of the receiver. For example, at the height of 0.5 m, 1 m, and 1.5 m, the mean 3D positioning error is 5.9 cm, 8.3 cm, and 14.2 cm, respectively. Thus, when the receiver is at a lower location, it tends to get a more accurate 3D positioning result. The reason is that lower PDs have larger distances to LEDs, thus enhancing their tolerance against the ranging error. On the right of Figure 5, we show the bird-eye view of the 3D positioning results, i.e., 2D positioning results, for the test locations at the height of 1 m, wherein the mean positioning error is 6.9 cm, which can meet the needs of most location-based services.

By considering the test locations in the receiving plane at the height of 1 m in Figure 5, Figure 6a shows the simulated CDFs of the 3D positioning errors at different locations. We assume $\Delta d = 0.025$ m and compare the CDFs obtained by adopting different intervals l between PDs. As can be seen, due to the same reason as in Figure 4, increasing l can effectively improve the overall positioning accuracy in the considered receiving plane. Specifically, when l is 0.1 m, 0.2 m, 0.5 m, and 1 m, around 90% of 3D positioning errors are less than 44.9 cm, 28.4 cm, 13.2 cm, and 7.9 cm, respectively. Therefore, to achieve a targeted positioning accuracy for the proposed VLPO scheme, we may appropriately increase the interval between PDs while considering the size of a receiver terminal. Take the shopping scenario as an example, with the proposed VLPO scheme, by installing a pair of PDs with

their interval to be 0.5 m on a shopping cart, we may achieve accurate 3D positioning for a customer with 92.7% of 3D positioning errors less than 20 cm using only two LEDs.

Corresponding to Figure 6a, Figure 6b plots the simulated CDFs of the azimuthal errors by considering the test locations in the receiving plane at the height of 1 m in Figure 5. We assume $\Delta d = 0.025$ m and compare the CDFs obtained by using different l . It is found that increasing l can effectively improve the overall orienteering accuracy in the considered receiving plane. The reason is the same as in Figure 6a. Specifically, around 77.7%, 87.4%, 91.6%, and 92.8% of azimuthal errors are less than 3° when l is 0.1 m, 0.2 m, 0.5 m, and 1 m, respectively, thereby verifying the high orienteering accuracy of the proposed VLPO scheme at different locations.

Based on the test locations in Figure 6, Figure 7 compares the mean positioning errors and azimuthal errors versus different standard derivations Δd of the distance estimation errors caused by ranging. We set $\Delta d = 0.0125$ m, 0.025 m, 0.05 m, and 1 m, and plot the mean positioning errors and azimuthal errors obtained by using different intervals l between PDs. The three curves above are the CDFs of mean azimuthal errors, and the three curves below are the CDFs of the mean azimuthal errors. We note that both the positioning accuracy and the orienteering accuracy degrade with an increased Δd . Specifically, when l is 0.5 m and Δd increases from 0.0125 m to 0.05 m, the mean positioning error increases from 3.5 cm to 15.2 cm, and the mean azimuthal error increases from 6.2° to 8.1° . Further, when Δd reaches 0.1 m, the mean positioning error is as large as 30.5 cm, which is inapplicable for high-accurate location-based services, whereas the mean azimuthal error is 11.2° . Thus, compared with the orienteering accuracy, the positioning accuracy is more sensitive to the distance estimation error between LEDs and PDs. Additionally, when Δd is stabilized at 0.025 m, the mean positioning error is 7.4 cm and the mean azimuthal error is 7.0° when l is 0.5 m. Therefore, high ranging accuracy is crucial to achieve the high-accurate performance of the proposed VLPO scheme.

Next, we evaluate the performance of the VLPO scheme when the receiver is tilted ($\theta > 0^\circ$). Figure 8a shows the simulated CDFs of the 3D positioning errors when the receiver is located at (1.5, 2, 1) with its polar angle θ fixed at 30° . We assume $\Delta d = 0.025$ m and use different curves to represent the CDFs obtained by adopting different intervals l between PDs. It can be seen that, when l is 0.1 m, 0.2 m, 0.5 m and 1 m, the probability of achieving 3D positioning errors less than 15 cm is 70.5%, 78.1%, 83.8%, and 85.7%, respectively, thereby verifying the effectiveness of the proposed VLPO scheme for a tilted receiver. Besides, a total of around 80% of 3D positioning errors are less than 28.5 cm when l is 0.1 m, and by further increasing l to 0.5 m, 80% of 3D positioning errors are less than 8.9 cm. Therefore, for the scenario of receiver tilt, adopting a larger l can effectively enhance the 3D positioning accuracy of the proposed VLPO scheme.

By using the same the simulated conditions as in Figure 8a, Figure 8b plots the simulated CDFs of the azimuthal errors. We see that when l is 0.1 m, 0.2 m, 0.5 m and 1 m, the probability of achieving azimuthal errors less than 5° is 89.5%, 93.1%, 95.2%, and 95.3%, respectively, thus proving the high orienteering accuracy of the proposed VLPO scheme for a tilted receiver. Furthermore, increasing the interval between PDs can enhance the orienteering accuracy effectively. For example, by increasing l from 0.1 m to 0.5 m, the probability of achieving azimuthal errors less than 3° can be improved from 79.4% to 93.4%, when $\theta = 30^\circ$.

To evaluate the performance of the VLPO scheme at different locations for a tilted receiver, Figure 9 shows an example of 3D positioning results in different receiving planes at the height of 0.5 m, 1 m, and 1.5 m. We fix the receiver polar angle θ at 20° to ensure that the LOS channels between LEDs and PDs will not be blocked due to the receiver tilt. We assume the interval between PDs is 0.2 m and the standard derivation Δd of the ranging error is 0.025 m. The test locations are the same as in Figure 5. On the left of Figure 9, we observe that most of the estimated 3D coordinates are close to their corresponding real locations, thus verifying the effectiveness of the proposed VLPO scheme at different locations for a tilted receiver. Specifically, the mean 3D positioning error is 9.2 cm, 14.2 cm,

and 20.9 cm at the height of 0.5 m, 1 m, and 1.5 m, respectively, from which the positioning accuracy is related to the height of the receiver. The reason is the same as in Figure 5. On the right of Figure 9, we show the corresponding 2D positioning results with a tilted receiver at the height of 1 m, wherein the mean positioning error is 10.7 cm. Besides, it can be observed that small positioning errors have a higher possibility to occur at the test locations below LEDs, e.g., where $x_R = 0$. This is because, when the receiver is tilted and located at the boundary of the considered indoor space with $x_R = 0$, multiple solutions of the estimated coordinates of PD₁ and PD₂ may stay close due to geometrical symmetry, thus their midpoints, i.e., the estimated locations of the receiver, have a higher chance to overlap, which potentially enhances the positioning accuracy at the test locations with $x_R = 0$.

By considering the test locations in the receiving plane at the height of 1 m in Figure 9, Figure 10a shows the simulated CDFs of the 3D positioning errors at different locations. We assume the standard derivation Δd of the ranging error is 0.025 m and the interval l between PDs is 0.5 m. We use different curves to represent the CDFs obtained by considering different polar angles with θ to be 0°, 10°, and 20°. For a performance evaluation, we also plot the simulated CDF curves of the 3D positioning errors when excluding the test locations below LEDs with $x_R = 0$. We see that increasing the polar angle of a tilted receiver slightly degrades the overall positioning accuracy in the considered receiving plane. Specifically, when θ is 0°, 10°, and 20°, the probability of achieving 3D positioning errors less than 20 cm is 92.7%, 90.3%, and 87.9%, respectively. In contrast, when excluding the test locations with $x_R = 0$, the probability of achieving 3D positioning errors less than 20 cm decreases to 91.5%, 88.7%, and 86.0% when θ is 0°, 10°, and 20°, respectively. By comparison, smaller positioning errors tend to occur at the test locations below LEDs with $x_R = 0$, which confirms the conclusion in Figure 9.

Corresponding to Figure 10a, Figure 10b plots the simulated CDFs of the azimuthal errors by considering the test locations in the receiving plane at the height of 1 m in Figure 9. We assume the standard derivation Δd of the ranging error is 0.025 m and the interval l between PDs is 0.2 m, and compare the CDFs obtained by considering different polar angles θ of the tilted receiver. It is found that increasing θ slightly degrades the overall orienteering accuracy in the considered receiving plane. Specifically, around 92.6%, 92.6%, and 90.9% of azimuthal errors are less than 5° when θ is 0°, 10°, and 20°, respectively, thereby verifying the high orienteering accuracy of the VLPO scheme at different locations for a tilted receiver. Moreover, when excluding the test locations with $x_R = 0$, around 99.5%, 99.2%, and 97.7% of azimuthal errors are less than 5° when θ is 0°, 10°, and 20°, respectively. Obviously, large azimuthal errors tend to occur at the test locations with $x_R = 0$. The reason lies in that, when the receiver tilts, although multiple solutions of the estimated coordinates of PD₁ and PD₂ may stay close due to geometrical symmetry as discussed in Figure 9, the estimated azimuthal angles of the receiver are completely different and their sum is 180°, thus degrading the orienteering accuracy at the test locations with $x_R = 0$.

Finally, based on the test locations in Figure 10, Figure 11 compares the mean positioning errors and azimuthal errors versus different polar angles θ of the tilted receiver. We assume $\Delta d = 0.025$ m. We set $\theta = 0^\circ, 10^\circ, \text{ and } 20^\circ$, and plot the mean positioning errors and azimuthal errors obtained by using different intervals l between PDs. As can be seen, the change in the polar angle of the tilted receiver has only a small influence on both the positioning accuracy and the orienteering accuracy. Specifically, when l is 0.2 m and θ changes from 0° to 20°, the mean positioning error slightly increases from 12.5 cm to 13.3 cm, and the mean azimuthal error slightly increases from 7.4° to 7.7°. Therefore, the proposed VLPO scheme is robust to the variation of the receiver polar angle, and can achieve stable 3D positioning and orienteering accuracy with a tilted receiver.

4. Conclusions

To enable indoor VLP when the LED condition is constrained, we proposed a novel 3D VLP and orienteering (VLPO) scheme. By using only two LEDs and a pair of PDs, the

scheme can simultaneously estimate the 3D coordinate and the orientation of the receiver. To support VLPO for a tilted receiver, we further proposed a location selection strategy to overcome the location uncertainty caused by receiver tilt. Simulation studies showed that, when the receiver faces upwards, the proposed VLPO scheme can achieve a mean 3D positioning error of 7.4 cm and a mean azimuthal error of 7.0° . Moreover, when the receiver tilts with a polar angle of 10° , the proposed scheme can still achieve accurate VLP with 90.3% of 3D positioning errors less than 20 cm, and accurate receiver orienteering with 92.6% of azimuthal errors less than 5° . The evaluation also indicated that appropriately increasing the interval between PDs can help enhance the tolerance against the ranging error, thus improving the VLPO accuracy effectively. In the future work, we will study and improve the VLPO scheme under scenarios when the LOS channels between LEDs and PDs are partially blocked.

Author Contributions: Conceptualization, X.Y. (Xiaodi You); methodology, X.Y. (Xiaodi You) and Z.J.; validation, X.Y. (Xiaodi You) and X.Y. (Xiaobai Yang); investigation, X.Y. (Xiaobai Yang) and S.Z.; resources, X.Y. (Xiaodi You); data curation, X.Y. (Xiaobai Yang); writing—original draft preparation, X.Y. (Xiaodi You); writing—review and editing, X.Y. (Xiaodi You); visualization, Z.J. and S.Z.; supervision, X.Y. (Xiaodi You); project administration, X.Y. (Xiaodi You); funding acquisition, X.Y. (Xiaodi You). All authors have read and agreed to the published version of the manuscript.

Funding: This research was funded by National Natural Science Foundation of China (62001319); Suzhou Science and Technology Bureau-Technical Innovation Project in Key Industries (SYG2021112); and Open Fund of IPOC (BUPT) (IPOC2020A009).

Institutional Review Board Statement: Not applicable.

Informed Consent Statement: Not applicable.

Data Availability Statement: Not applicable.

Conflicts of Interest: The authors declare no conflict of interest.

References

1. Liu, H.; Darabi, H.; Banerjee, P.; Liu, J. Survey of wireless indoor positioning techniques and systems. *IEEE Trans. Syst. Man Cybern. Part C-Appl. Rev.* **2007**, *37*, 1067–1080. [\[CrossRef\]](#)
2. Hassan, N.U.; Naeem, A.; Pasha, M.A.; Jadoon, T.; Yuen, C. Indoor positioning using visible led lights: A survey. *ACM Comput. Surv.* **2015**, *48*, 1–32. [\[CrossRef\]](#)
3. Luo, J.; Fan, L.; Li, H. Indoor positioning systems based on visible light communication: State of the art. *IEEE Commun. Surv. Tutor.* **2017**, *19*, 2871–2893. [\[CrossRef\]](#)
4. Campo-Jimenez, G.d.; Perandones, J.M.; Lopez-Hernandez, F.J. A VLC-based beacon location system for mobile applications. In Proceedings of the 2013 International Conference on Localization and GNSS (ICL-GNSS), Turin, Italy, 25–27 June 2013; pp. 1–4. [\[CrossRef\]](#)
5. Zhou, Z.; Kavehrad, M.; Deng, P. Indoor positioning algorithm using light-emitting diode visible light communications. *Opt. Eng.* **2012**, *51*, 0850091–0850096. [\[CrossRef\]](#)
6. Liu, Z.; You, X.; Wei, Z.; Wang, Z.; Li, M.; Chen, J.; Fu, H.Y.; Yu, C. Asynchronous visible light positioning based on orthogonal pseudo-random codes. In Proceedings of the 26th Optoelectronics and Communications Conference (OECC), Hong Kong, China, 3–7 July 2021; pp. 1–3. [\[CrossRef\]](#)
7. Zheng, H.; Xu, Z.; Yu, C.; Gurusamy, M. A 3-D high accuracy positioning system based on visible light communication with novel positioning algorithm. *Opt. Commun.* **2017**, *396*, 160–168. [\[CrossRef\]](#)
8. Nadeem, U.; Hassan, N.U.; Pasha, M.A.; Yuen, C. Indoor positioning system designs using visible LED lights: Performance comparison of TDM and FDM protocols. *Electron. Lett.* **2015**, *51*, 72–74. [\[CrossRef\]](#)
9. Chen, J.; You, X. Visible light positioning and communication cooperative systems. In Proceedings of the 2017 16th International Conference on Optical Communications and Networks (ICOON), Wuzhen, China, 7–10 August 2017; pp. 1–3. [\[CrossRef\]](#)
10. Al-Ahmadi, S.; Maraqa, O.; Uysal, M.; Sait, S.M. Multi-user visible light communications: State-of-the-art and future directions. *IEEE Access* **2018**, *6*, 70555–70571. [\[CrossRef\]](#)
11. Yang, H.; Chen, C.; Zhong, W.; Alphones, A.; Zhang, S.; Du, P. Demonstration of a quasi-gapless integrated visible light communication and positioning system. *IEEE Photonics Technol. Lett.* **2018**, *30*, 2001–2004. [\[CrossRef\]](#)
12. Zhang, B.; Zhang, M.; Ghassemlooy, Z.; Han, D.; Yu, P. A visible light positioning system with a novel positioning algorithm and two LEDs. In Proceedings of the 24th Optoelectronics and Communications Conference (OECC) and 2019 International Conference on Photonics in Switching and Computing (PSC), Fukuoka, Japan, 7–11 July 2019; pp. 1–3. [\[CrossRef\]](#)

13. Li, H.; Huang, H.; Xu, Y.; Wei, Z.; Yuan, S.; Lin, P.; Wu, H.; Lei, W.; Fang, J.; Chen, Z. A fast and high-accuracy real-time visible light positioning system based on single LED lamp with a beacon. *IEEE Photonics J.* **2020**, *12*, 7906512. [[CrossRef](#)]
14. Liu, Z.; You, X.; Chen, J.; Yu, C. Two-LED indoor visible light positioning method based on channel estimation with a mirror. In Proceedings of the 2019 Asia Communications and Photonics Conference (ACP), Chengdu, China, 2–5 November 2019; pp. 1–3.
15. Hao, J.; Chen, J.; Wang, R. Visible light positioning using a single LED luminaire. *IEEE Photonics J.* **2019**, *11*, 1–13. [[CrossRef](#)]
16. You, X.; Liu, Z.; Gao, M.; Chen, J.; Yu, C.; Shen, G. Indoor three-dimensional optical wireless positioning and orienteering using steerable line lasers. In Proceedings of the 2020 Asia Communications and Photonics Conference (ACP) and International Conference on Information Photonics and Optical Communications (IPOC), Beijing, China, 24–27 October 2020; pp. 1–3.
17. Yang, S.; Kim, H.; Son, Y.; Han, S. Three-dimensional visible light indoor localization using AOA and RSS with multiple optical receivers. *J. Light. Technol.* **2014**, *32*, 2480–2485. [[CrossRef](#)]
18. Zhou, B.; Liu, A.; Lau, V. Joint user location and orientation estimation for visible light communication systems with unknown power emission. *IEEE Trans. Wirel. Commun.* **2019**, *18*, 5181–5195. [[CrossRef](#)]
19. Shen, S.; Li, S.; Steendam, H. Simultaneous position and orientation estimation for visible light systems with multiple LEDs and multiple PDs. *IEEE J. Sel. Areas Commun.* **2020**, *38*, 1866–1879. [[CrossRef](#)]
20. Yang, X.; Jiang, Z.; You, X.; Chen, J.; Yu, C.; Li, Y.; Gao, M.; Shen, G. A 3D visible light positioning and orienteering scheme using two LEDs and a pair of photo-detectors. In Proceedings of the 2021 Asia Communications and Photonics Conference (ACP), Shanghai, China, 24–27 October 2021; pp. 1–3. [[CrossRef](#)]
21. Wang, T.Q.; Sekercioglu, Y.A.; Neild, A.; Armstrong, J. Position accuracy of time-of-arrival based ranging using visible light with application in indoor localization systems. *J. Light. Technol.* **2013**, *31*, 3302–3308. [[CrossRef](#)]
22. Zhang, S.; Zhong, W.; Du, P.; Chen, C. Experimental demonstration of indoor sub-decimeter accuracy VLP system using differential PDOA. *IEEE Photonics Technol. Lett.* **2018**, *30*, 1703–1706. [[CrossRef](#)]
23. You, X.; Chen, J.; Yu, C. Performance of location-based equalization for OFDM indoor visible light communications. *IEEE Trans. Cogn. Commun. Netw.* **2019**, *5*, 1229–1243. [[CrossRef](#)]
24. Jiang, Z.; You, X.; Shen, G.; Mukherjee, B. Location-aware spectrum sensing for cognitive visible light communications over multipath channels. *Opt. Express* **2021**, *29*, 43700–43719. [[CrossRef](#)]